Journal of NAMP 70, (2025) 143-154

The Nigerian Association of Mathematical Physics

Journal homepage: https://nampjournals.org.ng

SMS FIBER TEMPERATURE SENSORS USING OPTICAL TIME-DOMAIN REFLECTOMETRY

[1]Osaisai, D. T, [2]Awodu, O., [3]Suleiman, A. S., and [2]Azi, S. O

[1]Physics Department, Faculty of Science, Niger Delta University, Amassoma, Bayelsa State
[2]Department of Physics, University of Benin, Benin City
[3]Department of Physics with Electronics, Auchi Polytechnic, Auchi..

ARTICLE INFO

Article history:
Received 15/6/2025
Revised 2/7/2025
Accepted 11/7/2025
Available online 17/7/2025

Keywords:
SMS fiber-optic temperature sensors; Ghost phenomena; Optical Time-Domain Reflectometry (OTDR).

ABSTRACT

This paper presents a detailed analysis of ghost phenomena observed in Optical Time-Domain Reflectometry (OTDR) traces of Single-mode–Multimode–Single-mode (SMS) fiber temperature sensors. A theoretical model based on modal interference and temperature-dependent phase shifts is developed, and experimental studies are carried out using an Anritsu MT9083A2 OTDR system. The combined analysis links temperature changes with the dynamics of ghost peaks. The findings demonstrate how pulse width and temperature affect device performance, providing valuable insights for optimizing fiber-optic sensor applications.

1. INTRODUCTION

Optical fiber sensors have been widely adopted due to their immunity to electromagnetic interference, high sensitivity, and suitability for distributed and remote sensing. They are the basis of the design and analysis of fiber optic and filters. Among various sensor configurations, Single-mode–Multimode–Single-mode (SMS) fiber structures have accelerated research interest due to their versatile applications in optical sensing, signal processing, and laser technology [1-3]. Theoretical investigations into multimode interference (MMI) in Single-Mode–Multimode–Single-Mode (SMS) fiber structures have been extensively conducted using various modeling approaches. These include beam propagation methods (BPM) [4, [5], ray-tracing techniques [6], [7] and numerical simulations implemented in COMSOL Multiphysics [8] and MATLAB [9-11]. These studies form the theoretical foundation of the complex modal behavior and interference mechanisms in SMS structures.

*Corresponding author: AZI, S. O.
E-mail address: ogochukwuazi@uniben.edu
https://doi.org/10.60787/jnamp.vol69no2.538

While theoretical models offer valuable insights into the performance of SMS-based fiber systems, their precision is often limited by the inherent complexities of light propagation, modal interference, and the influence of external perturbations. Experimental validations have further confirmed the sensitivity and effectiveness of SMS structures in practical scenarios [1], [2], [7], [12].

Recent literature reviews [13], [14] suggest that ongoing research in advanced materials, innovative fiber geometries, and advanced signal processing algorithms improves the applicability of SMS-based devices across diverse sensing applications. SMS fiber structures have already demonstrated high sensitivity in a wide range of measurement devices including: vibration [15], [6], strain [17], [18], [19], temperature [20-22], refractive index [11], [23], [24] magnetic fields [25], [26], displacement [1], salinity [27], weight [28], acoustics [29], flow rate [2], and ascorbic acid detection [30]. These achievements underscore the versatility and potential of SMS structures in fiber-optic sensing technology, motivating continued research and development in this field.

Light pulses launched from a single-mode fiber (SMF) excite multiple propagation modes within a multimode fiber (MMF), resulting in an interference pattern in the output single-mode fiber. The generated wavelength-dependent output peaks and dips are due to modal interference. Consequently, “Ghosts” are observed between and beyond the length of the fiber cable. These ghost effects arise from modal interference, imperfect coupling between modes, or the re-excitation of higher-order modes within the multimode fiber. The term “ghost phenomena” in SMS fiber structures typically refers to interference artifacts, side lobes, or unexpected spectral features in their transmission profiles. This phenomenon originates from any of the three processes: *unwanted residual coupling to higher-order modes, Fabry–Pérot effects and **a**symmetric or non-adiabatic transitions*. Fabry-Perot interference is of particular interest in this work as it can be located beyond the fiber cable.

(SMS) Sensors, when integrated with Optical Time-Domain Reflectometry (OTDR), enable distributed sensing with localized interrogation along extended fiber links. A distinctive phenomenon observed in OTDR traces of SMS sensors is *ghost peaks,* spurious reflection signals that do not correspond to actual physical discontinuities. These artifacts are sensitive to temperature variations and are attributed to modal interference and refractive index mismatches within the multimode fiber segment between the fiber cable lengths. Rayleigh backscattering in single-mode fibers follows a well-defined path, whereas interference from propagation modes in multimode fibers results in complex backscatter profiles [31]. Interactions between different modes create multiple optical paths with differing time delays, which the OTDR may misinterpret as ghost peaks [32[, [33].

Ghosts typically appear at predictable distances relative to major reflection events, yet standard OTDR analysis techniques often struggle to distinguish them from real reflections. As temperature increases, the intensity of ghost peaks tends to diminish slightly, and their positions shift due to thermal expansion and changes in the refractive index [20[, [22]. Several studies have reported the presence of ghost artifacts in SMS structures, linking them to modal interference and differential group delays in the multimode sections [34]. Others, however, proposed methods to suppress the "ghost" phenomenon observed in OTDR traces of SMS fiber structures. Nonetheless, investigation of changes in temperature-dependent refractive index and modal propagation on ghost signals beyond SMS optical fiber links is scarce in the literature. As a result, the underlying physics is poorly understood.

Furthermore, existing models rarely incorporate the modal dynamics that affect the fidelity of OTDR signals in SMS fiber sensors [35]. False reflections by ghosts beyond the fiber cable link are misleading and complicate the interpretation of OTDR traces of SMS-based temperature sensors. This paper presents an initial study on ghost reflections observed in the OTDR transmission profiles of SMS fiber sensors under varying temperature conditions.

2. THEORETICAL BACKGROUND

2.1 Multimode Interference

In single-mode-multimode-single-mode (SMS) fibers, (MMI) plays a critical role [36]. The light exiting the first single-mode fiber excites multiple modes in the multimode fiber section.

$$E_{SMF}(r,0) = \sum_m A_m \Psi_m(r) \quad (1)$$

where A_m is the modal excitation coefficient for the m-th LP mode, $\psi_m(r)$ is the transverse mode These modes interfere with each other, creating a complex spatial distribution that evolves as the light propagates. At certain distances, self-imaging occurs, where the input field profile is reproduced [3]. The equations governing MMI relate the input field to the field at a distance *z* along the multimode fiber, assuming a weakly guiding approximation, the electric field in MMF can be expressed as a superposition of Linearly Polarized modes [37],

$$E_{MMF}(r,z) = \sum_m A_m \Psi_m(r) e^{j\beta_m z} \quad (2)$$

where A_m is the modal excitation coefficient for the $m-th$ LP mode, $\psi_m(r)$ is the transverse mode profile, β_m is the propagation constant of the m-th mode and z is the propagation distance along the MMF which is determined by the overlap integral between $E(r,0)$ and $\Psi_m(r)$ as [37]

$$A_m = \frac{\int_0^\infty E(r,0)\Psi_m(r)dr}{\int_0^\infty \Psi_m(r)\Psi_m(r)dr} \quad (3)$$

After propagating through length L in the multimode fiber, the output field is given as;

$$E_{OUT}(r) = \sum_m A_m \Psi_m(r) e^{j\beta_m L} \quad (4)$$

The output SMF couples to this field via the same overlap integral in Equation (3) when the output is symmetrically coupled to the MMF. The intensity distribution at the output SMF is given by the superposition of these modes [15[, [38].

$$I(x,y,L) = \left| \sum_{m=1}^{M} A_m \psi_m(x,y) e^{j\beta_m L} \right|^2 \quad (5)$$

where *I(x, y, L)* is the intensity distribution at a distance along the MMF, and *L* is the length of the MMF section. Equation (5) relates the output intensity to the interference of the multiple modes, and the phase shift is critical in altering the modal interference pattern. [37].

2.2 Ghost Formation Physics

Ghosts in SMS structures are caused by [38]:

a. Beats between modes

The interference between non-fundamental $m-th$ and $n-th$ modes with similar propagation constants introduce secondary interference fringes:

$$\Delta\beta_{mn} = \beta_m - \beta_{nm} \quad (6)$$

and the wavelength as

$$\Lambda_{mn} = \frac{2\pi}{\Delta\beta_{mn}} \quad (8)$$

These additional periods can appear as ghost peaks in the spectral response.

b. Imperfect Mode Matching

If the launch conditions or alignment are not optimal, weak excitation of unintended modes causes multiple low-intensity interference terms and incoherent additive effects in the output.

c. Back-reflections and Fabry–Pérot effects

Reflections at SMF-MMF interfaces or poorly cleaved ends can form Fabry–Pérot cavities, generating secondary resonances.

2.3 Temperature Dependence of Modal Propagation

The propagation constant β_m of the $m-th$ mode is given by [39], [40]:

$$\beta_m = \frac{2\pi n_m}{\lambda} \quad (9)$$

where n_m is the effective refractive index of the $m-th$ mode and λ is the wavelength of the light. The temperature dependence of the effective refractive index can be expressed as:

$$\frac{dn_m}{dT} = \frac{\delta n_m}{\delta T} + \frac{\delta n_m}{\delta \lambda}\frac{d\lambda}{dT} \quad (10)$$

where $\frac{\delta n_m}{\delta T}$ is the thermo-optic coefficient, which represents the change in refractive index with temperature, and $\frac{\delta n_m}{\delta \lambda}\frac{d\lambda}{dT}$ accounts for the wavelength dependence of the refractive index and the thermal expansion of the fiber. The change in the phase difference between two modes, $\Delta\varphi_m = (\beta_m - \beta_n)L$. A change in temperature ΔT can be approximated as:

$$\Delta\varphi_{mn} \approx \frac{2\pi L}{\lambda}\left(\frac{dn_m}{dT} - \frac{dn_n}{dT}\right)\Delta T \quad (11)$$

where L is the length of the MMF section. OTDR can detect this change in phase difference arising from a shift in the interference pattern.

2.4 OTDR Signal Analysis

OTDR backscatter measurement is a nondestructive method and requires access to only one end of the fiber to determine optical fiber attenuation. The injected pulse into the test fiber and return signals are measured as a function of time. Ghost peaks in OTDR traces of SMS sensors are caused by nonlinear phase shifts between propagating modes, resulting in constructive interference at unexpected positions along the fiber. The phase condition that determines the apparent location of ghosts is [41].

$$\Delta\varphi_m(z) = 2\pi k, \quad k \in Z \tag{12}$$

This condition causes the reinforcement of backscattered light at points where no physical reflector occurs. The OTDR measures the backscattered light as a function of time. The backscattered power $P(z)$ at a distance z at the input end of the fiber is given by:

$$P(z) = P_0 S \alpha_s W e^{(-2\alpha z)} \tag{13}$$

where P_0 is the launch power, S is the backscatter capture fraction, α_S is the Rayleigh scattering coefficient, W is the pulse width, and α is the attenuation coefficient of the fiber. In the presence of an SMS fiber sensor, the OTDR signal will exhibit a loss peak at the location of the MMF section due to modal interference. Equation (10) describes the sensitivity of the depth and shape of this loss peak to temperature changes. By analyzing the changes in the OTDR signal, the ambient temperature can be determined.

3. EXPERIMENTAL SETUP

An Anritsu MT9083A2 OTDR operating at 1550 nm was used to acquire OTDR traces from the SMS fiber sensor. The sensor consists of a 5 cm multimode fiber (MMF) spliced between two single-mode fibers (SMF), with interconnecting patch panels. The system was configured with a pulse width of 50 ns for most measurements

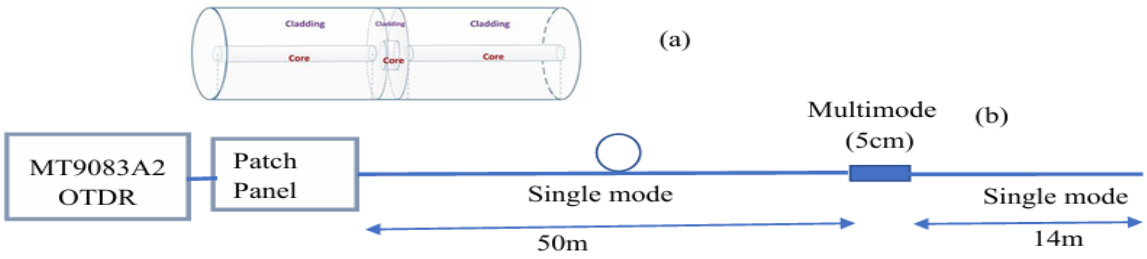

Figure 3.1: Experimental setup for temperature measurement (a) SMS structure, (b) Optic Fiber setup.

OTDR traces were acquired in three temperature regimes: Low temperatures from 0.3°C to 7.9°C, near room temperatures between 8.2°C and 20.0°C, and at elevated temperatures from 28.9°C to 68.3°C. A separate set of traces with a 20 ns pulse width was recorded between 4.1°C and 19.7°C to analyze the interference fringes (ghosts) with higher spatial resolution. It is pertinent to note here light pulses were launched continuously in a swept mode with an interval of thirty seconds. The fiber sensor was gradually heated by pulsed laser radiation.

RESULTS AND DISCUSSION

OTDR traces at different temperatures were superimposed in a Yokogawa AQ7933 trace viewer. The ghost peaks showed that the backscattered signal from the SMS structure exhibited temperature dependence. The depth and shape of extended peaks varied randomly with temperature. Thus, it is not straightforward to determine the temperature sensitivity. Resolution of the sensor was limited by the noise floor of the OTDR and the stability of the laser source. The peculiarities of the three temperature regimes are discussed as follows.

4.1. Analysis of OTDR traces in the low temperature regime

Figure 4.1 shows an overlay of all OTDR traces recorded in the low-temperature regime. Four prominent interference peaks, each roughly 20 meters apart, appeared beyond the fiber trunk's endpoint at 64 meters. The first event, at 46 meters, corresponds to a ghost reflection labeled G1 at 92 meters. A splice loss at 55 m created a corresponding ghost, G2, at 110 meters. The reflection from the fiber end at 64 meters generated a ghost G3 at 130 meters. Additionally, a minor reflection at 76 meters produced G4 at 152 meters. These ghost peaks, G1, G2, G3, and G4, occur at approximately twice the distances of their associated physical events, consistent with ghost phenomena described in OTDR reference manuals [42], [43] and scholarly articles [23], [24].

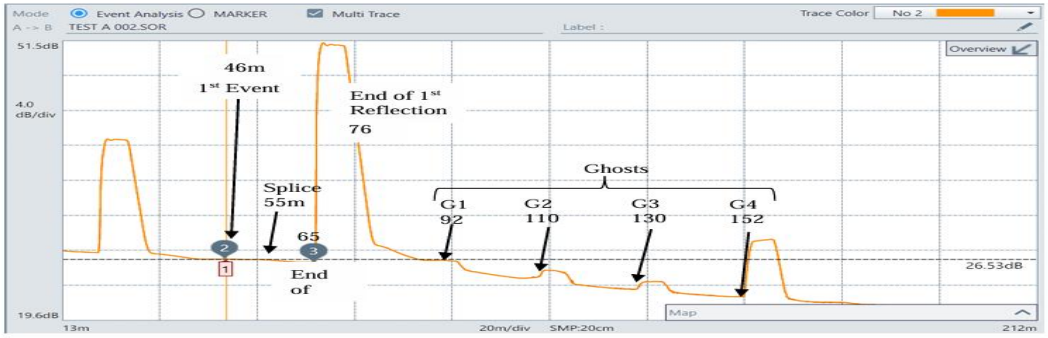

Figure 4.2: Full OTDR trace of SMS fiber with 50 ns pulse width at 1550 nm at low temperatures (-0.3°C to 7.9°C).

The peaks at G3 and G4 were enlarged in Figure 4.3 to highlight the OTDR traces at various temperatures. In Figure 4.3b, the traces appear noisy and interleaved. The lowest signal level at 23.3 dB reads 0.7°C, while the highest indicates 2.4°C at 23.7 dB. Intermediate traces, representing temperatures from –0.3 °C to 6.3 °C, appeared in no particular order. This random or non-monotonic temperature dependence complicates the interpretation of OTDR data in SMS temperature sensors. Although the traces in Figure 4.3b are smoother, they exhibited the same irregularity, with both the lowest and highest signals corresponding to 2.4 °C at 29.2 dB and 0.7°C at 30.0 dB. A comparison of Figures 4.3a and 4.3b revealed that the trace direction differs between them.

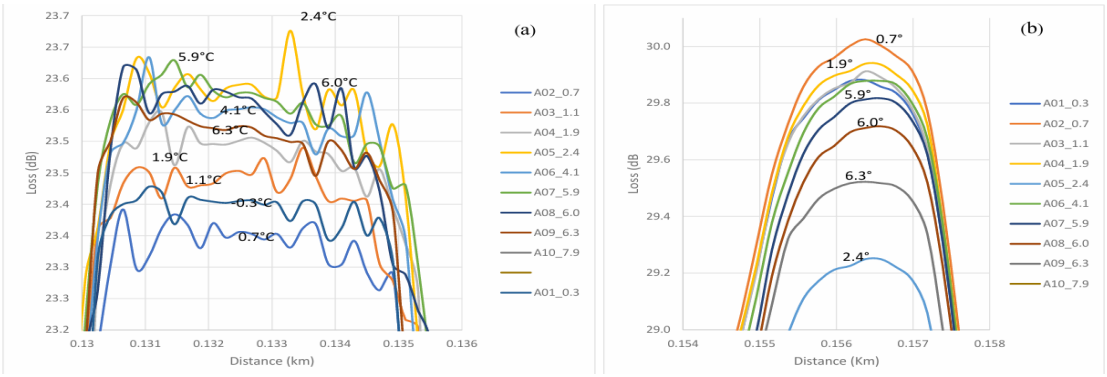

Figure 4.2: OTDR traces and magnified peak of traces with 50 ns pulse width at 1550 nm at low temperatures (-0.3°C to 7.9°C). (a) Overlapped traces at G3. (b) Overlapped traces G4.

4.2. OTDR traces at near room temperature regime

The superimposition of all traces at the near-room-temperature regime is shown in Figure 4.3a. Only overlapping peaks at G4 were expanded in Figure 4.3b to emphasize the OTDR traces at various temperatures. The respective lowest and highest signal levels are 30.1 dB at 10.8°C and

28.8 dB at 17.1°C. Intermediate traces representing temperatures between 8.2 °C and 19.9 °C appear at random signal levels. Here, the interpretation of OTDR data traces is confounded by non-monotonic temperature dependence. It is pertinent to mention that the other peaks showed the same broad, unpredictable characteristics

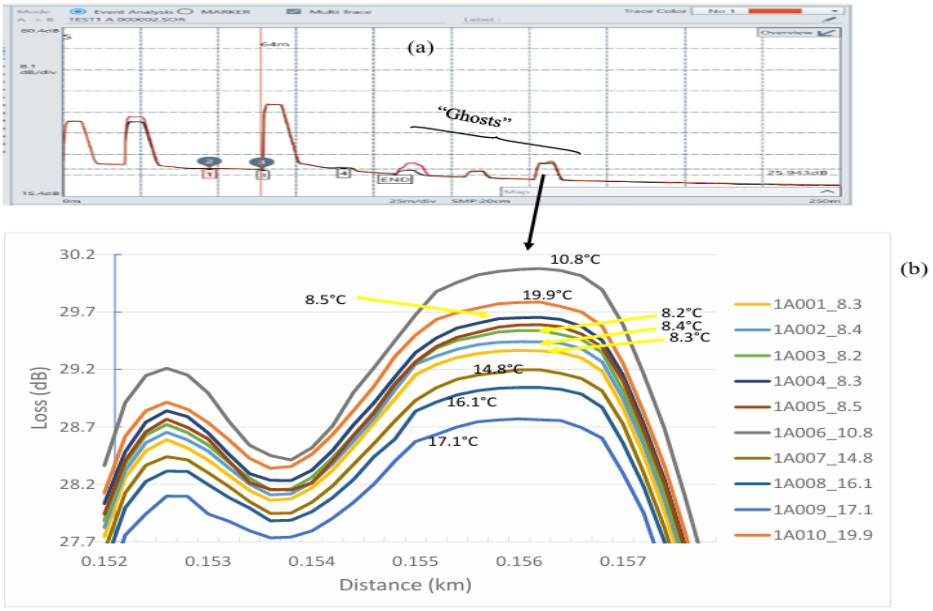

Figure 4.3: OTDR traces and magnified peak of traces with 50 ns pulse width at 1550 nm between 8.2°C and 19.9°C.

4.3. OTDR traces at elevated temperatures

The only ghost peak in Figure 4.4 was extended to highlight the OTDR traces at higher temperatures. The traces were quite broad, with the lowest signal level at 24.5 dB read 28.9°C, while the highest indicated 29.8 dB at 68.3°C. Intermediate traces, representing temperatures between this 38°C range, are not in any particular order. Again, the anomaly in temperature dependence complicates the interpretation of OTDR data. Further investigation would be required to unravel why only one peak is displayed in these traces.

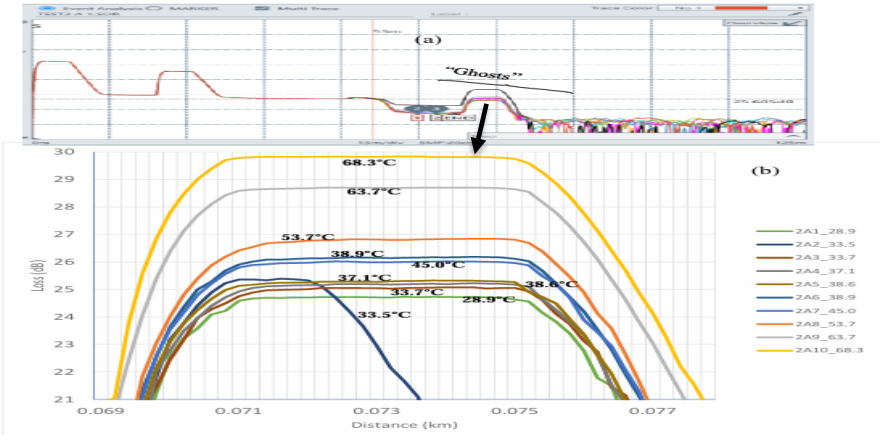

Figure 4.4: OTDR traces and magnified peak of traces with 50 ns pulse width at 1550 nm at elevated temperatures (28.9°C to 68.3°C).

4.4. OTDR traces at low temperatures with 20ns pulse

Five traces between 4.1 °C and 19.7 °C were superimposed in Figure 4.5a. Four more peaked ghosts were recorded. The peak at G4 was expanded in Figure 4.5b to emphasize the OTDR traces at measured temperatures. The respective lowest and highest signal levels are 30.5 dB at 4.1°C and 27.9 dB at 19.7°C. Intermediate traces representing temperatures are monotonic and appear to follow a downward trend. The interpretation OTDR data traces here showed clear temperature dependence, with narrow peaks. Only four temperatures were recorded in this figure. It will be of interest to include many more temperature points.

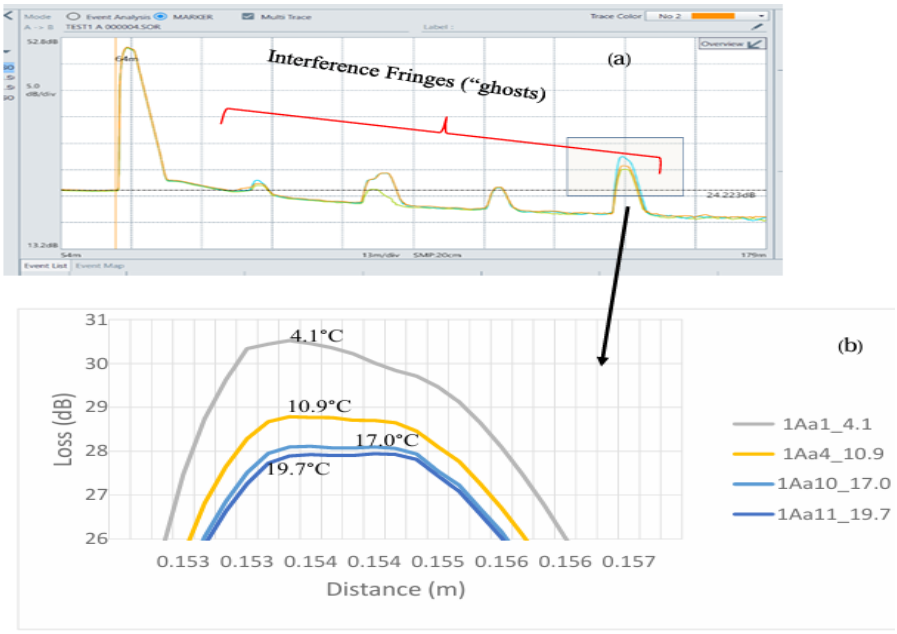

Figure 4.5: OTDR traces and magnified peak of traces with 20 ns pulse width at 1550 nm between 4.1°C and 19.7°C.

A summary of the temperature ranges and ghost peak characteristics is presented in Table 4.1. Experimental OTDR traces recorded at given temperatures revealed that ghost peaks vary in intensity, spacing, and shape. At low temperatures, the contrast between the primary reflection and ghost peaks is more pronounced, while at higher temperatures, the ghost peaks become broader and less distinct. A comparison of traces with 50 ns and 20 ns pulse widths demonstrates that shorter pulse widths increase spatial resolution, giving a clearer distinction between true reflections and ghost signals. These findings are consistent with the theoretical model of ghost formation due to phase shifts induced by temperature variations.

Table 4.1: Summary of Temperature Ranges, Pulse Widths, and Observations

Temperature Range (°C)	Pulse Width (ns)	Peak Base (m)	Max. Loss (Range (dB))	Observations
-0.3 to 7.9	50	5	28.7 (0.8)	Distinct ghost peaks with high intensity; sharper modal interference.

8.2 to 19.9	50	6	30.1(1.3)	Ghost peaks shift and broaden with temperature rise.
28.9 to 68.3	50	9	29.8 (5.3)	Ghost dynamics are evident with gradual intensity reduction.
4.1 to 19.7	20	3	30.5 (2.5)	Enhanced resolution of interference fringes; fine details of ghost patterns observed.

CONCLUSION

This paper provides a theoretical explanation for the ghost phenomena observed in OTDR traces of SMS fiber temperature sensors. Through a combination of modal interference theory and experimental analysis, it is shown that temperature-induced phase shifts play a critical role in the formation of ghost peaks. Experimental results acquired using the Anritsu MT9083A2 OTDR confirm that both the pulse width and operating temperature have a significant impact on sensor performance. Future efforts will focus on optimizing sensor design to enhance rather than minimize ghost effects and improve overall measurement accuracy.

REFERENCES

[1] Wu, Q., Qu, Y., Liu, J., Yuan, J., Wan, S.-P., Wu, T., He, X.-D., Liu, B., Liu, D., Ma, Y., Semenova, Y., Wang, P., Xin, X., & Farrell, G. (2021). Singlemode-Multimode-Singlemode Fiber Structures for Sensing Applications—A Review. *IEEE Sensors Journal*, *21*(11), 12734–12751. https://doi.org/10.1109/jsen.2020.3039912A

[2] Olivero M, Bellone A, Bano A, Vallan A and Perrone G (2022), Optical fiber flowmeter based on a single mode multimode-single mode structure. Front. Sens. 3:985963. doi: 10.3389/fsens.2022.985963

[3] Morshed, A. H. E., and Shalaby, M. Y. (2014). Bending characteristics of single mode-Multimode-Single mode optical fiber structures. *2014 31st National Radio Science Conference (NRSC)*, 303–310. https://doi.org/10.1109/nrsc.2014.6835090.

[4] Chuprov, I., Efremenko, D., Gao, J., Anisimov, P., & Zemlyakov, V. (2022). Scaling transformation of the multimode nonlinear Schrödinger equation for physics-informed neural networks (Version 1). arXiv. https://doi.org/10.48550/ARXIV.2209.14641

[5] Wong, N. H. L., Jung, Y., Alam, S., Petropoulos, P., & Richardson, D. J. (2017). Numerical analysis of mode propagation and coupling in multimode fibers. 2017 Opto-Electronics and Communications Conference (OECC) and Photonics Global Conference (PGC), 1–3. https://doi.org/10.1109/oecc.2017.8115029

[6] Geok, T., Hossain, F., Kamaruddin, M., Abd Rahman, N., Thiagarajah, S., Tan Wee Chiat, A., Hossen, J., Liew, C., A Comprehensive Review of Efficient Ray-Tracing Techniques for Wireless Communication, (2018) *International Journal on Communications Antenna and Propagation (IRECAP)*, 8 (2), pp. 123-136. doi:https://doi.org/10.15866/irecap.v8i2.13797

[7] Wang, K., Xingchen Dong, X., Michael H. Kohler, M. H., Kienle, P., Bian, Q., Jakobi,M., and Alexander W. Koch (2020), IEEE SENSORS JOURNAL, VOL. XX, NO. XX, XXXX DOI 10.1109/JSEN.2020.3015086

[8] Younus, S. I., Al-Dergazly, A. A., & Abass, A. K. (2021). Characterization of Multimode Interference Based Optical Fiber. *IOP Conference Series: Materials Science and Engineering*, *1076*(1), 012060. https://doi.org/10.1088/1757-899x/1076/1/012060

[9] Hu, S., Hu X., Li J., He Y., Qin H, Li S., Liu M., Liu C., Zhao C., and Chen W. (2024). "Enhancing Vibration Detection in ϕ-OTDR Through Image Coding and Deep Learning-Driven Feature Recognition," *IEEE Sensors Journal*, vol. 24 (22) pp. 38344-38351, **DOI:** 10.1109/JSEN.2024.3469232

[10] K. Yao, Q. Lin, Z. Jiang, N. Zhao, B. Tian and G. -D. Peng, "Design and Analysis of a Combined FBG Sensor for the Measurement of Three Parameters," in *IEEE Transactions on Instrumentation and Measurement*, vol. 70, pp. 1-10,

[11] *Veettikazhy, M., Kragh Hansen, A., Marti, D., Mark Jensen, S., Lykke Borre, A., Ravn Andresen, E., Dholakia, K., & Eskil Andersen, P. (2021). BPM-Matlab: an open-source optical propagation simulation tool in MATLAB. Optics Express, 29(8), 11819. https://doi.org/10.1364/oe.420493*

[12] Barrias A., Joan R. Casas J. R., and Villalba S. (2016)A Review of Distributed Optical Fiber Sensors for Civil Engineering Applications. Sensors, 16, p748-; doi:10.3390/s16050748

[13] Ma, C.; Peng, D.; Bai, X.; Liu, S.; Luo, L. A Review of Optical Fiber Sensing Technology Based on Thin Film and Fabry–Perot Cavity. Coatings 2023, 13, 1277. https:// doi.org/10.3390/coatings13071277)

[14] Yu Z F, Li Y F, Guo M L, Luo B., Luo X., and Geng D. (2025). A Brief Review of Optical Fiber Sensor based on Multimode Interference. J. Study on Optical Communications, 247, pp 1-8. DOI：10.13756/j.gtxyj.2025.230177

[15] Waluyo T. B., and Bayuwati D. (2017) J. Phys.: Conf. Ser. 817 012035

[16] Egorov, F. A., & Potapov, V. T. (2012). Optical fiber vibration measuring transducers based on irregular multimode fibers. *Technical Physics Letters*, *38*(6), 527–530. https://doi.org/10.1134/s106378501206003x

[17] Sun, Y., Liu, D., Lu, P., Sun, Q., Yang, W., Wang, S., Liu, L. and Ni, W. (2017). High sensitivity optical fiber strain sensor using twisted multimode fiber based on SMS structure. Optics Communications, 405, 416–420. https://doi.org/10.1016/j.optcom.2017.08.059

[18] Lalam, N., Ng, W. P., Wu, Q., Dai, X., & Fu, Y. Q. (2016). Perfluorinated polymer optical fiber for precision strain sensing based on novel SMS fiber structure. 2016 10th International Symposium on Communication Systems, Networks and Digital Signal Processing (CSNDSP), 1–3. https://doi.org/10.1109/csndsp.2016.7573938

[19] Biswas, R. (2020). Inexpensive Hetero-core Spliced Fiber Optic Setup for Assessing Strain. *Sensing and Imaging*, *21*(38). https://doi.org/10.1007/s11220-020-00298-z

[20] Sakata, H., Okada, K., & Mochizuki, J. (2021). Highly sensitive temperature sensor based on multimode-interference fiber structure with gel cladding. *Microwave and Optical Technology Letters*, *63*(6), 1647–1651. https://doi.org/10.1002/mop.32823

[21] Olivero, M., Vallan, A., Orta, R., and Perrone, G. (2018). Singlemode multimode-single mode optical fiber sensing structure with quasi-two-mode fibers. IEEE Trans. Instrum. Meas. 67 (5), 1223–1229. doi:10.1109/tim.2017. 2771998

[22] Zhang, W., Lu, Y., & He, C. (2024). High-accuracy high temperature measurement based on forward Brillouin scattering of polyimide-coated optical fiber. *Optical Fiber Technology*, *83*, 103653. https://doi.org/10.1016/j.yofte.2023.103653

[23] Liu, Z., Yu, M., Huang, S., Liu, X., Wang, Y., Liu, M., Pan, P. and Liu, G. (2015) Enhancing refractive index sensing capability with hybrid plasmonic–photonic absorbers, J. Mater. Chem. C. Vol. 3, 17, pp4222-4226

[24] Liu, J.-D., Kari, N., Liu, H.-S., Wang, W.-S., Xia, Z.-M., & Wang, Q. (2024). Highly Sensitive Multimode-Single-Mode-Multimode Optical Fiber SPR Refractive Index Sensor with GaSe Nanosheets. *Plasmonics*, *20*(1), 167–178. https://doi.org/10.1007/s11468-024-02252-1

[25] Chen, Y., Han, Q., Liu, T., Lan, X., & Xiao, H. (2013). Optical fiber magnetic field sensor based on single-mode–multimode–single-mode structure and magnetic fluid. *Optics Letters*, *38*(20), 3999. https://doi.org/10.1364/ol.38.003999

[26] Ascorbe, J., Corres, J. M., Arregui, F. J., & Matias, I. R. (2015). Magnetic field sensor based on a single mode-multimode-single mode optical fiber structure. *2015 IEEE SENSORS*, 1–4. https://doi.org/10.1109/icsens.2015.7370226

[27] Li, A., Dai, L., Li, S., Zhang, Y., Lewis, E., Wang, S., Wang, P., & Yin, Y. (2024). Simultaneous salinity and temperature measurement using multimode interference effect. *Optical Fiber Technology*, *84*, 103691. https://doi.org/10.1016/j.yofte.2024.103691

[28] Liu, Y., and Cai, L. (2019). An optical fiber weight sensor based on SMS fiber structure. In Z. Li (Ed.), *17th International Conference on Optical Communications and Networks (ICOCN2018)* (p. 11). SPIE. https://doi.org/10.1117/12.2518290

[29] Sun, A., Semenova, Y., & Farrell, G. (2010). A novel highly sensitive optical fiber microphone based on single mode–multimode–single mode structure. *Microwave and Optical Technology Letters*, *53*(2), 442–445. https://doi.org/10.1002/mop.25688

[30] Gupta, V. K., Choudhary, K., and Kumar, S. (2024). Ascorbic Acid Detection Using Gold Nanoparticles and Graphene Oxide–Coated SMS Optical Fiber–Based Sensor. Plasmonics. https://doi.org/10.1007/s11468-024-02577-x

[31] Agrawal, G. P. (2019). Nonlinear Fiber Optics, Academic Press https://doi.org/10.1016/C2011-0-00045-5

[32] Aydin D., Barnes J. A., and Loock H. (2023). *Appl. Phys. Rev.* 10 (1), 011307 https://doi.org/10.1063/5.0105147

[33] Lee, T., Kim, E. and Park, J. (2007). Implementation methods of repetitive sampling on an OTDR for alignment of ghost reflection in short-period measurement with a short-length fiber, Optical Fiber Technology, Vol. 13 (3). 246-253, ttps://doi.org/10.1016/j.yofte.2007.03.002.

[34] K. Tian, X. Wang, G. Farrell, and P. Wang, "Single-Mode-Multimode-Single-Mode Fibre Structure for Sensing Applications: A Review," in *Advanced Photonics 2018 (BGPP, IPR, NP, NOMA, Sensors, Networks, SPPCom, SOF)*, OSA Technical Digest (online) (Optica Publishing Group, 2018), paper SeM4E.1.

[35] Cai L, Liu Y, Hu S, Liu Q. Optical fiber temperature sensor based on modal interference in multimode fiber lengthened by a short segment of polydimethylsiloxane. *Microw Opt Technol Lett*. 2019; 61: 1656–1660. https://doi.org/10.1002/mop.31843

[36] Yu, Z., Yong-xing, J., and Shang-zhong, J. (2011). Numerical simulation of spectral transmission characteristics of single-mode-multimode-single-mode fiber structure. In *Journal of China University of Metrology*

[37] Wang, Q., Farrell, G. and Yan W, (2008). Investigation on Single-Mode–Multimode–Single-Mode Fiber Structure. Journal of Lightwave Technology, Vol. 26, no. 5, pp. 512-519

[38] Bhatia N.and John, J. (2014). Multimode interference devices with single-mode–multimode–multimode fiber structure. Appl. Opt. vol. 53, pp 5179-5186. https://opg.optica.org/ao/abstract.cfm?URI=ao-53-23-5179

[39] Sirin, S., Aldogan, K. Y. and Wuilpart, M. (2022). "Current sensing using a Phase-Sensitive Optical Time Domain Reflectometer: Feasibility study," Optical Fiber Technology, vol. 76, p. 102663. https://doi.org/10.1016/j.yofte.2022.103084.

[40] Adilkhanova, A., Nurlankyzy, M., Kazhiyev, S., Blanc, W., Bekmurzayeva, A. and Daniele Tosi, D. (2024). "Fiber optic refractive index sensing using an inline dual semi-distributed interferometer," Optik, vol. 306, p. 167865, https://doi.org/10.1016/j.ijleo.2024.171713.

[41] Markvart A. A., Liokumovich L. B., & Ushakov N. A. (2022). Fiber Optic SMS Sensor for Simultaneous Measurement of Strain and Curvature. Technical Physics Letters, *48*(15), 30. https://doi.org/10.21883/tpl.2022.15.53817.18969

[42] Hayes J. (2019). Ghosts and Goblins: How OTDRs Work, Part 4. https://www.ecmag.com/magazine/articles/article-detail/integrated-systems-Ghosts and Goblins: How OTDRs Work, Part 4

[43] Thereza M. M. Giraldi R. Cindy S. Fernandes, C. S., Ferreira, M. S., Marco J. de Sousa, M. J., Pedro Jorge, P., Costa, J. C. W. A., Jose L. Santos, J. L., and Frazao O. (2015). Fiber Optic Displacement Sensor based on a Double-Reflecting OTDR Technique. Microwave and Optical Technology Letters. Vol. 57 (6). Pp 1312-1315. DOI 10.1002/mop